ISSN 0021-3640, JETP Letters, 2023, Vol. 117, No. 5, pp. 363–369. © The Author(s), 2023. This article is an open access publication.
Russian Text © The Author(s), 2023, published in Pis'ma v Zhurnal Eksperimental'noi i Teoreticheskoi Fiziki, 2023, Vol. 117, No. 5, pp. 369–376.

CONDENSED MATTER

Joint Intercalation of Ultrathin Fe and Co Films under a Graphene Buffer Layer on a SiC(0001) Single Crystal

S. O. Filnov[a,*], D. A. Estyunin[a], I. I. Klimovskikh[a,c], T. P. Makarova[a], A. V. Koroleva[a], A. A. Rybkina[a], R. G. Chumakov[b], A. M. Lebedev[b], O. Yu. Vilkov[a], A. M. Shikin[a], and A. G. Rybkin[a]

[a] *St. Petersburg State University, St. Petersburg, 198504 Russia*

[b] *National Research Center Kurchatov Institute, Moscow, 123182 Russia*

[c] *Center for Promising Methods of Mesophysics and Nanotechnologies, Moscow Institute of Physics and Technology (National Research University), Dolgoprudnyi, Moscow region, 141701 Russia*

**e-mail: sfilnov@gmail.com*

Received November 14, 2022; revised January 29, 2023; accepted January 29, 2023

The joint intercalation of Co and Fe atoms under a graphene buffer layer synthesized on a SiC(0001) single crystal has been studied. Intercalation has been performed by means of the alternating deposition of ultrathin Fe and Co metal films on the substrate heated to 450°C with the subsequent heating to 600°C in 15 min. It has been shown that Co and Fe atoms under these conditions are intercalated under graphene, forming compounds with silicon and with each other. The existence of a magnetic order in the system up to room temperature has been demonstrated using a superconducting quantum interferometer. A possible stoichiometry of the formed alloys has been analyzed using data on the shape and magnitude of hysteresis loops. In addition, it has been found that Fe and Co in the system exposed to the atmosphere are not oxidized. Thus, graphene protects the formed system. This study makes contribution to the investigation of graphene in contact with magnetic metals and promotes its application in spintronic and nanoelectronic devices.

DOI: 10.1134/S0021364022603025

1. INTRODUCTION

The study and modification of the properties of graphene are attractive for various scientific fields because of numerous unique electronic and structural characteristics of graphene-based systems [1–5]. It is predicted theoretically that fundamental effects such as the spin-dependent Seebeck effect [6], quantum spin and anomalous Hall effects [7, 8], and superconductivity [9, 10] can be observed in graphene. The ballistic transport of electrons in graphene [11, 12] and a large spin relaxation length [13, 14] allow numerous concepts of spintronic and nanoelectronic graphene-based devices [15, 16].

Numerous effects are based on the interaction of graphene with magnetic materials. In particular, the combination of spin–orbit and exchange interactions induced in graphene by, e.g., the proximity effect can lead to the quantum anomalous Hall effect, which is of both fundamental and applied interests [8, 17, 18]. Because of a strong σ bond, graphene placed between two magnetic conductors can be used as a barrier in devices involving a magnetic tunnel transition [16]. A large spin relaxation length makes it possible to use graphene as a channel for spin-polarized electrons in spin transistors [16, 19].

Thus, the study of graphene on magnetic substrates requires special attention. However, for the subsequent application in spintronic and nanoelectronic devices, a system should be synthesized on an insulating or semiconducting substrate. This can be achieved by chemical deposition from a gas phase on a metallic substrate [20–28] with the subsequent transfer on the insulating substrate or by the thermal graphitization of SiC with a low charge carrier density [29–32]. The latter method is more favorable because it does not require additional transfer, which worsens the transport characteristics of graphene [12, 33]. To induce magnetism in the Gr/SiC system (Gr is graphene), a layer of magnetic atoms is formed between graphene and SiC by means of intercalation. Some studies were devoted to Gr/MM/SiC systems (MM is a magnetic metal), where atoms of transition (Fe, Co) [34–39] and rare-earth (Eu, Dy, Gd, Er) [40–42] metals were used as intercalated elements. However, despite a quite high magnetic ordering temperature in pure compounds of these elements, the resulting systems have a paramagnetic or ferromagnetic order with a low magnetic ordering temperature compared to ordering temperature in bulk samples of these elements. A possible reason for such a behavior in Gr/MM/SiC systems can be the formation of compounds of intercalated metals with silicon. Silicides thus formed usually have

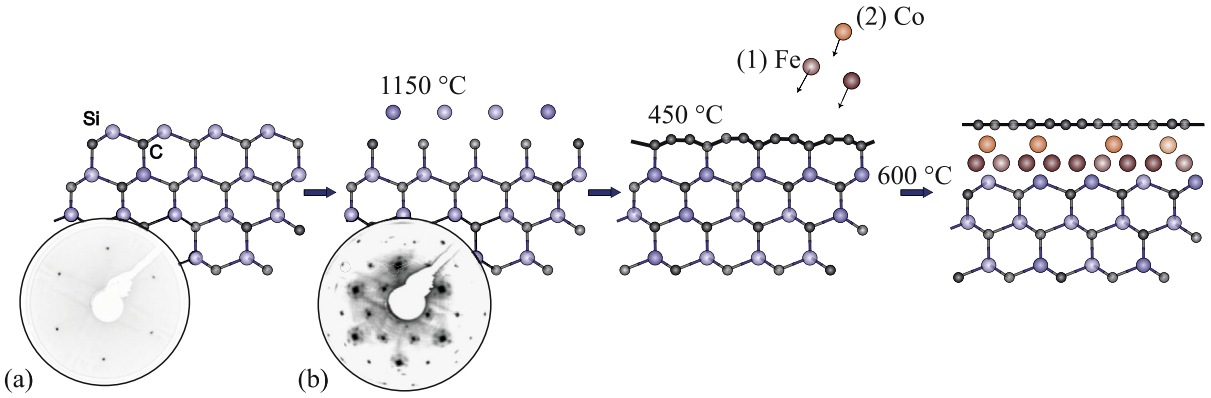

Fig. 1. (Color online) Sketch of the synthesis of the Gr/Fe–Co/SiC system. Low-energy electron diffraction patterns for (a) the initial 6H-SiC(0001) surface and (b) the $(6\sqrt{3}\times 6\sqrt{3})R30^\circ$ reconstruction of the SiC surface after annealing at a temperature of 1150°C.

a paramagnetic or low-temperature ferromagnetic order [43–45].

The authors of [39] showed that the intercalation of a cobalt film thicker than 1 nm under graphene on SiC leads to a change in the intensity of photoemission spectra for the Co3*p* level under the variation of the magnetization of the sample, which can indicate the ferromagnetic ordering of the intercalated layer. In [34], we showed that the intercalation of the ultrathin Co film under the graphene buffer layer on SiC results in the transformation of the graphene buffer layer to a graphene monolayer and in the formation of an ultrathin magnetic cobalt silicide layer, where magnetism is due to the low-lying CoSi layer. However, the absence of magnetic ordering at room temperature limits the application of this system in spintronic devices. The authors of [35] studied the effect of the intercalation of iron atoms on the properties of the Gr/SiC system. Density functional theory calculations and angle-resolved photoelectron spectroscopy measurements showed that Fe atoms can affect the spin polarization of the π band in bilayer graphene. It was also found that graphene prevents the oxidization of iron in the Gr/Fe/SiC system exposed to the atmosphere [38], which is important for the stability of the magnetic properties in the final system. However, the experimental study of the magnetic properties of this system is still required.

The aim of this work is to examine the magnetic properties and the electronic structure of a system obtained after the joint intercalation of ultrathin Fe and Co films under the graphene buffer layer synthesized on the Si termination of the SiC(0001) single crystal. We used semi-insulating 6H-SiC(0001) single crystal plates with a resistivity of $\rho = 10^5$ Ω/cm. The synthesis of the graphene buffer layer was controlled by low-energy electron diffraction. The electronic structure was studied by X-ray photoelectron spectroscopy (XPS). The XPS experimental data were also used to estimate the distribution of elements over the depth in the resulting system. The magnetic properties of the system were examined by a SQUID.

2. EXPERIMENTAL RESULTS AND DISCUSSION

Figure 1 presents the sketch of the synthesis of the system and low-energy electron diffraction measurements before and after the synthesis of the graphene buffer layer. To synthesize the graphene buffer layer, the thermal graphitization of the Si-terminated surface of 6H-SiC(0001) was used at the first stage. The initial single crystal had the 1 × 1 hexagonal surface structure typical of SiC(0001) (see Fig. 1a). Heating to 1150°C leads to the appearance of a moiré structure around the main reflections or the so-called $(6\sqrt{3}\times 6\sqrt{3})R30^\circ$ structure, which indicates the formation of the graphene buffer layer on the surface [31, 32, 46] (see Fig. 1b). At the next stage of the formation of the system, 14-Å-thick iron and 7-Å-thick cobalt films were alternatingly deposited by means of physical vapor-phase deposition on the substrate heated to 450°C with the subsequent heating to 600°C in 15 min after each deposition. As shown in [34, 36, 38], this method is appropriate for the intercalation of both Fe and Co atoms.

To analyze the formed system, we carried out XPS measurements at different detection angles of photoelectrons. Figure 2 shows the measurements of core levels of the system. Spectra were analyzed by decomposition into spectral components. The C1*s* spectrum has a two-component form. The component with a higher binding energy (285 eV) corresponds to C atoms in graphene obtained at the rupture of bonds between the graphene buffer layer and the substrate because of the intercalation of metal atoms [31, 32, 34]. The component with a lower binding energy (283.3 eV) corresponds to C atoms in the SiC sub-

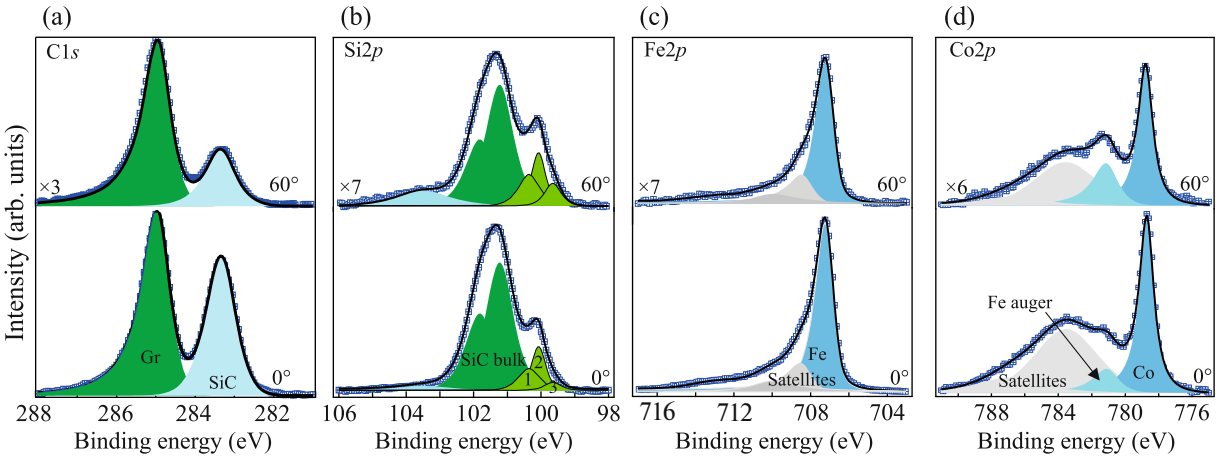

Fig. 2. (Color online) X-ray photoelectron spectra measured at a photon energy of 1486.6 eV and an electron detection angle of (top panels) 60° and (bottom panels) 0°.

strate. The Si2p level is decomposed into six peaks. Two peaks shown in dark green correspond to silicon in the SiC substrate, three peaks shown in light green assumingly correspond to metal silicides [34, 36, 38, 39, 47], and the left 103.6-eV peak corresponds to SiO_2 [48, 49]. The Fe2$p_{3/2}$ level is decomposed into three components: the main component shown in blue and satellites characteristic of the ground levels of metals. At the same time, the Co2p level has a more complex structure. In addition to the main component with the lowest binding energy, there are three components. Components assumingly responsible for satellites are shown in gray. The Fe Auger peak, which is in this range at this photon energy, is shown in turquoise.

To determine the relative order of deposition of the elements under the assumption that their distribution is planar and uniform, we comparatively analyzed the ratios I_{60}/I_0 of the intensities of XPS spectral components measured at angles of incidence of 60° and 0° (see Table 1). For convenience, the data are given in units of the intensity of the C1s graphene component (285 eV). The SiO_2 compound is the nearest to the surface. This fact can be explained by a feature of the formation of graphene during the thermal graphitization of silicon carbide. In [34], clusters, assumingly silicon, which are formed because of the heating of the SiC single crystal above 1000°C, were detected on atomic force microscopy images of the surface of SiC after the formation of the graphene buffer layer. Since XPS spectra were recorded after the transfer of the system to ambient conditions, we assume that SiO_2 clusters are present on the surface of graphene. The analysis shows that the upper layer in the formed system is graphene (Gr component). Iron and cobalt silicides (Si_1, Si_2, and Si_3 components) are localized under graphene. It is noteworthy that the stoichiometry of the synthesized metal silicides cannot be unambiguously determined from the data obtained because the peaks of the Si2p level corresponding to the Co–Si and Fe–Si compounds are close in binding energy [50, 51]. However, comparison with the published data shows that the formation of the $CoSi_2$ and FeSi compounds is the most probable [34, 47, 50, 51]. According to the data summarized in Table 1, Co and Fe metals lie below. Iron is located deeper because it was deposited earlier than cobalt. The deepest element in the system is silicon in the SiC substrate. These data confirm the intercalation of Fe and Co atoms under the graphene buffer layer with the formation of the graphene monolayer, cobalt silicide, iron silicide, and possibly the Fe–Co compound between graphene and substrate.

We also note that features associated with oxides are absent in the spectra of iron and cobalt [52]; i.e., intercalated metals in the system transferred to ambient conditions are not oxidized, which is important for the application of such systems in spintronic devices. The authors of [38] also found that graphene prevents

Table 1. Ratios of the intensities of the spectral components of X-ray photoelectron spectra measured at different angles of emission of photoelectrons

Peak	Binding energy, eV	I_{60}/I_0
SiO_2	103.6	1.5
Gr	285	1.
Si_3	99.7	0.8
Si_2	100.1	0.65
Si_1	100.4	0.64
Co	778.8	0.45
Fe	707.25	0.4
Si bulk	101.6	0.4

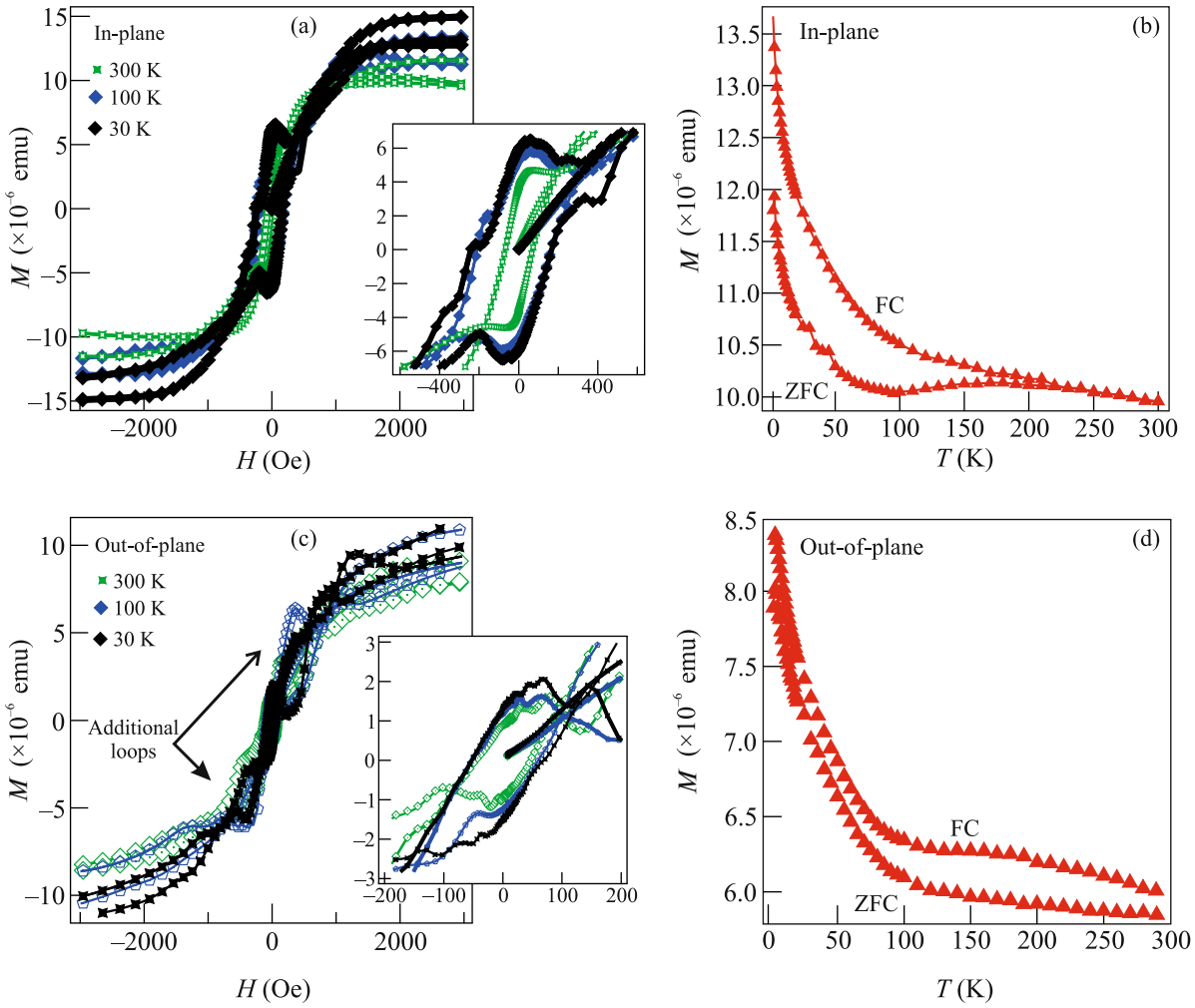

Fig. 3. (Color online) (a, c) Isothermal magnetization curves $M(H)$ of the synthesized system at different temperatures and (b, d) the temperature dependence of the magnetization $M(T)$ under cooling (ZFC) in zero field and (FC) in a magnetic field of $H = 1$ kOe.

the oxidization of iron intercalated under graphene on SiC.

To study the magnetic properties of the system, we measured the magnetization as a function of the temperature and the applied magnetic field using a SQUID magnetometer. Figures 3a and 3b show the dependences of the magnetic moment of the sample on the applied magnetic field and the temperature, respectively, measured in the sample plane. The magnetic field dependence $M(H)$ demonstrates a hysteresis loop up to room temperature, which indicates ferromagnetic or ferrimagnetic ordering in the system. The shape of the hysteresis loop with characteristic magnetization jumps in the region ±200 Oe is similar to the shape of the hysteresis loop detected for ferromagnetic FeSi polycrystalline films on silicon [53]. Figure 3b demonstrates that the FC and ZFC curves diverge at a temperature of about $T = 240$ K. This behavior is inherent in supermagnets [54–57] and indicates the presence of superferromagnetic particles having a superspin, which is the sum of individual magnetic moments of atoms inside a particle [57]. It is known that some iron and cobalt silicides that are nonmagnetic in bulk can manifest ferromagnetic properties in ultrathin films and nanowires [53, 58, 59]. However, the shape of the hysteresis loop in our case differs from that in the case of magnetic nanothin CoSi [59]; furthermore, the Si2*p* spectrum (Fig. 2b) does not include the typical features of CoSi [34]. In combination with the characteristic magnetization jumps on the dependence $M(H)$, this allows us to assume that ferromagnetic ordering is determined by FeSi.

Analyzing the dependences of the magnetization $M(H)$ and $M(T)$ in the direction perpendicular to the surface of the sample, we reveal several unique features. First, the presence of the hysteresis loop on $M(H)$ curves at all temperatures indicates ferromag-

netic or ferrimagnetic ordering in this direction. Second, in addition to the main hysteresis loop, Fig. 3c demonstrates secondary hysteresis loops. A similar behavior of $M(H)$ with secondary hysteresis loops for ultrathin layers of magnetic compounds was detected in [60], where it was attributed to different exchange interactions in neighboring layers. It is also seen that the ZFC and FC $M(T)$ curves do not coincide in the entire temperature range under study. However, they are similar to the ZFC and FC curves in Fig. 3b below the point of divergence. It can be assumed that the temperature of divergence for this direction is higher than room temperature. The temperature of the magnetic transition can be different for the in-plane and out-of-plane directions because the exchange interaction is anisotropic in these directions.

A possible stoichiometry of the formed compounds can be analyzed in terms of coercive forces. The coercive force H_C for the in-plane direction in the formed system at room temperature is about 200 Oe, which is an order of magnitude larger than that in epitaxial ternary [61, 62] and binary [63] silicides. The magnetic properties of the synthesized system were compared to those of pure Co and Fe films in terms of coercive forces. The magnetic properties of thin Co and Fe films are strongly different from the properties of bulk ferromagnets. The coercive force depends on the thickness of a film, its epitaxy or polycrystallinity, and the substrate. The authors of [64] showed that the coercive force for ultrathin cobalt films with a thickness of 8–15 monolayers on a silicon substrate is about 40–100 Oe. The coercive force for ultrathin iron films deposited on the silicon surface at low temperature also does not exceed 100 Oe [65]. These coercive forces are much smaller than that observed for the system obtained in this work.

Thus, the formation of the FeSi and $CoSi_2$ compounds revealed in XPS data is confirmed by the presence of magnetization jumps on hysteresis loops characteristic of FeSi. The $CoSi_2$ compound is nonmagnetic even in the nanosamples and does not contribute to the magnetic properties. However, a coercive force of 200 Oe observed in the experiment at room temperature cannot be reached in any of the listed compounds. Consequently, the formation of compounds of iron and cobalt can be assumed because the coercive force for Fe–Co alloys at room temperature is about 200 Oe [66], which is in good agreement with the coercive force measured for our system. It is noteworthy that the coercive force and the shape of the hysteresis loop are determined to a great extent by the domain structure of the ferromagnet. The shape of the hysteresis loop strongly depends on the morphology and shape of crystallites in a polycrystal, as well as on their type and number [67, 68]. All these factors can strongly affect the coercive force H_C in the formed system. Since Fe–Co particles can be superferromagnetic [55], the formation of a Fe–Co alloy at the interface between graphene and the substrate is not excluded.

3. CONCLUSIONS

To summarize, a system obtained by means of the joint intercalation of ultrathin cobalt and iron films under a graphene buffer layer grown on a silicon carbide single crystal has been analyzed. Intercalation has been performed by means of the alternating deposition of ultrathin Fe and Co metal films on the substrate heated to 450°C with the subsequent heating to 600°C in 15 min. The analysis of X-ray photoelectron spectra has confirmed the formation of a graphene/Fe–Co/SiC system. It has also been found that intercalated metals form compounds with silicon (FeSi, $CoSi_2$) and with each other (Fe–Co). The existence of a magnetic order up to room temperature has been demonstrated using a SQUID magnetometer. The magnetic ordering temperature of the system obtained by the intercalation of only one of the elements (Fe or Co) under graphene on SiC does not exceed 100 K. A significant increase in the magnetic ordering temperature in the formed system is due to the formation of magnetic ultrathin layers of Fe–Co alloys under graphene. The formation of these alloys is evidenced by a wide (about 200 Oe) hysteresis loop on the $M(H)$ dependence at room temperature. It has also been shown that graphene protects the formed system. Indeed, iron and cobalt oxides are not observed in the formed system exposed to the ambient conditions. A small amount of SiO_2 is detected most probably because of the formation of Si clusters on the graphene surface and subsequent oxidation.

The proposed method for the formation of a graphene-containing system with a quite high magnetic ordering temperature can be used in some scientific and applied problems, e.g., in the study of the quantum anomalous Hall effect in graphene at high temperatures and thereby in its application in spintronic and nanoelectronic devices. The synthesized system can also be used to fabricate a spin transistor, where the magnetic alloy can serve as a "drain" for the generation of the spin current, whereas graphene having a long spin relaxation length can serve as a medium for the subsequent transfer of this current to the "source" of the transistor.

4. METHODS

Before synthesis, the sample was prepared by heating-induced degassing in ultrahigh vacuum at temperatures up to 800°C. The graphene buffer layer was synthesized by the graphitization of the silicon surface of the SiC(0001) single-crystal sample. The thicknesses of deposited iron and cobalt layers were controlled by means of the preliminary calibration of sources with XPS. The synthesis of the system and measurements of low-energy electron diffraction were

carried out at the NANOPES beamline of the Kurcharov Complex for Synchrotron and Neutron Investigations (National Research Center Kurchatov Institute) [69]. Preliminary works for the optimization of the synthesis technology were performed at the resource center Physical Methods of Surface Investigation, Research Park, St. Petersburg State University. Angle-resolved photoelectron spectroscopy measurements for the final system were carried out on an ESCALAB 250Xi photoelectron spectrometer, resource center Physical Methods of Surface Investigation, Research Park, St. Petersburg State University. The prepared system was transferred between the synthesis chamber and the measurement chamber under ambient conditions. The magnetic characteristics were measured at the resource center Center of Diagnostics of Functional Materials for Medicine, Pharmacology, and Nanoelectronics, Research Park, St. Petersburg State University, using a Quantum Design MPMS SQUID VSM magnetometer.

FUNDING

This study was supported by the Ministry of Science and Higher Education of the Russian Federation (project no. 94031444 for St. Petersburg State University) and by the Russian Science Foundation (project no. 18-12-00062). I.I. Klimovskikh acknowledges the support of the Ministry of Science and Higher Education of the Russian Federation (contract no. 075-02-2021-1316 dated September 30, 2021; Strategic Academic Leadership Program Priority 2030).

CONFLICT OF INTEREST

The authors declare that they have no conflicts of interest.

OPEN ACCESS

This article is licensed under a Creative Commons Attribution 4.0 International License, which permits use, sharing, adaptation, distribution and reproduction in any medium or format, as long as you give appropriate credit to the original author(s) and the source, provide a link to the Creative Commons license, and indicate if changes were made. The images or other third party material in this article are included in the article's Creative Commons license, unless indicated otherwise in a credit line to the material. If material is not included in the article's Creative Commons license and your intended use is not permitted by statutory regulation or exceeds the permitted use, you will need to obtain permission directly from the copyright holder. To view a copy of this license, visit http://creativecommons.org/licenses/by/4.0/.

REFERENCES

1. A. K. Geim and K. S. Novoselov, Nat. Mater. **6**, 183 (2007).
2. M. J. Allen, V. C. Tung, and R. B. Kaner, Chem. Rev. **110**, 132 (2010).
3. A. M. Shikin, V. K. Adamchuk, S. Siebentritt, K.-H. Rieder, S. L. Molodtsov, and C. Laubschat, Phys. Rev. B **61**, 7752 (2000).
4. A. M. Shikin, D. Farias, V. K. Adamchuk, and K. H. Rieder, Surf. Sci. **424**, 155 (1999).
5. S. K. Tiwari, S. Sahoo, N. Wang, and A. Huczko, J. Sci.: Adv. Mater. Dev. **5**, 1 (2020).
6. D.-D. Wu and H.-H. Fu, Nanotechnology **32**, 245703 (2021).
7. C. L. Kane and E. J. Mele, Phys. Rev. Lett. **95**, 226801 (2005).
8. P. Högl, T. Frank, K. Zollner, D. Kochan, M. Gmitra, and J. Fabian, Phys. Rev. Lett. **124**, 136403 (2020).
9. A. V. Fedorov, N. I. Verbitskiy, D. Haberer, C. Struzzi, L. Petaccia, D. Usachov, O. Y. Vilkov, D. V. Vyalikh, J. Fink, M. Knupfer, B. Büchner, and A. Grüneis, Nat. Commun. **5**, 3257 (2014).
10. B. M. Ludbrook, G. Levy, P. Nigge, et al., Proc. Natl. Acad. Sci. U. S. A. **112**, 11795 (2015).
11. X. Du, I. Skachko, A. Barker, and E. Y. Andrei, Nat. Nanotechnol. **3**, 491 (2008).
12. L. Banszerus, M. Schmitz, S. Engels, M. Goldsche, K. Watanabe, T. Taniguchi, B. Beschoten, and Ch. Stampfer, Nano Lett. **16**, 2 (2016).
13. M. Drögeler, Ch. Franzen, F. Volmer, T. Pohlmann, L. Banszerus, M. Wolter, K. Watanabe, T. Taniguchi, Ch. Stampfer, and B. Beschoten, Nano Lett. **16**, 3533 (2016).
14. M. Venkata Kamalakar, Ch. Groenveld, A. Dankert, and S. P. Dash, Nat. Commun. **6**, 6766 (2015).
15. S. Sato, Jpn. J. Appl. Phys. **54**, 4 (2015).
16. E. C. Ahn, npj 2D Mater. Appl. **4**, 17 (2020).
17. A. G. Rybkin, A. A. Rybkina, M. M. Otrokov, O. Yu. Vilkov, I. I. Klimovskikh, A. E. Petukhov, M. V. Filianina, V. Yu. Voroshnin, I. P. Rusinov, A. Ernst, A. Arnau, E. V. Chulkov, and A. M. Shikin, Nano Lett. **18**, 1564 (2018).
18. A. G. Rybkin, A. V. Tarasov, A. A. Rybkina, D. Yu. Usachov, A. E. Petukhov, A. V. Eryzhenkov, D. A. Pudikov, A. A. Gogina, I. I. Klimovskikh, G. di Santo, L. Petaccia, A. Varykhalov, and A. M. Shikin, Phys. Rev. Lett. **129**, 226401 (2022).
19. Y. G. Semenov, K. W. Kim, and J. M. Zavada, Appl. Phys. Lett. **91**, 15 (2007).
20. S. Bae, H. Kim, Y. Lee, et al., Nat. Nanotechnol. **5**, 574 (2010).
21. H. Ago, Y. Ito, N. Mizuta, K. Yoshida, B. Hu, C. M. Orofeo, M. Tsuji, K.-i. Ikeda, and S. Mizuno, ACS Nano **4**, 7407 (2010).
22. A. V. Fedorov, A. Yu. Varykhalov, A. M. Dobrotvorskii, A. G. Chikina, V. K. Adamchuk, and D. Yu. Usachov, Phys. Solid State **53**, 1952 (2011).
23. Y. Zhang, L. Zhang, and C. Zhou, Acc. Chem. Res. **46**, 2329 (2013).
24. D. Yu. Usachov, K. A. Bokai, D. E. Marchenko, A. V. Fedorov, V. O. Shevelev, O. Yu. Vilkov, E. Yu. Kataev, L. V. Yashina, E. Rühl, C. Laubschatf, and D. V. Vyalikh, Nanoscale **10**, 12123 (2018).
25. I. I. Klimovskikh, M. M. Otrokov, V. Yu. Voroshnin, D. Sostina, L. Petaccia, G. di Santo, S. Thakur, E. V. Chulkov, and A. M. Shikin, ACS Nano **11**, 368 (2017).

26. Y. Wang, F. Qing, Y. Jia, Y. Duan, Ch. Shen, Y. Hou, Y. Niu, H. Shi, and X. Li, Chem. Eng. J. **405**, 127014 (2021).
27. D. A. Estyunin, I. I. Klimovskikh, V. Yu. Voroshnin, D. M. Sostina, L. Petaccia, G. di Santo, and A. M. Shikin, J. Exp. Theor. Phys. **125**, 762 (2017).
28. M. M. Otrokov, I. I. Klimovskikh, F. Calleja, A. M. Shikin, O. Vilkov, A. G. Rybkin, D. Estyunin, S. Muff, J. H. Dil, A. L. Vázquez de Parga, R. Miranda, H. Ochoa, F. Guinea, J. I. Cerdá, E. V. Chulkov, and A. Arnau, 2D Mater. **5**, 035029 (2018).
29. C. Berger, Zh. Song, T. Li, X. Li, A. Y. Ogbazghi, R. Feng, Zh. Dai, A. N. Marchenkov, E. H. Conrad, Ph. N. First, and W. A. de Heer, J. Phys. Chem. B **108**, 19912 (2004).
30. M. G. Mynbaeva, A. A. Lavrent'ev, and K. D. Mynbaev, Semiconductors **50**, 138 (2016).
31. C. Riedl, C. Coletti, and U. Starke, J. Phys. D **43**, 374009 (2010).
32. K. V. Emtsev, F. Speck, T. Seyller, L. Ley, and J. D. Riley, Phys. Rev. B **77**, 155303 (2008).
33. D. de Fazio, D. G. Purdie, A. K. Ott, Ph. Braeuninger-Weimer, T. Khodkov, S. Goossens, T. Taniguchi, K. Watanabe, P. Livreri, F. H. L. Koppens, S. Hofmann, I. Goykhman, A. C. Ferrari, and A. Lombardo, ACS Nano **13**, 8926 (2019).
34. A. A. Rybkina, S. O. Filnov, A. V. Tarasov, D. V. Danilov, M. V. Likholetova, V. Yu. Voroshnin, D. A. Pudikov, D. A. Glazkova, A. V. Eryzhenkov, I. A. Eliseyev, V. Yu. Davydov, A. M. Shikin, and A. G. Rybkin, Phys. Rev. B **104**, 155423 (2021).
35. S. J. Sung, J. W. Yang, P. R. Lee, J. G. Kim, M. T. Ryu, H. M. Park, G. Lee, C. C. Hwang, K. S. Kim, J. S. Kima, and J. W. Chung, Nanoscale **6**, 3824 (2014).
36. S. O. Filnov, A. A. Rybkina, A. V. Tarasov, A. V. Eryzhenkov, I. A. Eliseev, V. Yu. Davydov, A. M. Shikin, and A. G. Rybkin, J. Exp. Theor. Phys. **134**, 188 (2022).
37. K. Shen, H. Sun, J. Hu, et al., J. Phys. Chem. C **122**, 37 (2018).
38. M. V. Gomoyunova, G. S. Grebenyuk, V. Yu. Davydov, I. A. Ermakov, I. A. Eliseyev, A. A. Lebedev, S. P. Lebedev, E. Yu. Lobanova, A. N. Smirnov, D. A. Smirnov, and I. I. Pronin, Phys. Solid State **60**, 1439 (2018).
39. G. S. Grebenyuk, E. Yu. Lobanova, D. A. Smirnov, I. A. Eliseyev, A. V. Zubov, A. N. Smirnov, S. P. Lebedev, V. Yu. Davydov, A. A. Lebedev, and I. I. Pronin, Phys. Solid State **61**, 1374 (2019).
40. N. A. Anderson, M. Hupalo, D. Keavney, M. C. Tringides, and D. Vaknin, Phys. Rev. Mater. **1**, 054005 (2017).
41. P. D. Bentley, T. W. Bird, A. P. J. Graham, O. Fossberg, S. P. Tear, and A. Pratt, AIP Adv. **11**, 025314 (2021).
42. N. A. Anderson, M. Hupalo, D. Keavney, M. Tringides, and D. Vaknin, J. Magn. Magn. Mater. **474**, 666 (2019).
43. V. N. Narozhnyi and V. N. Krasnorussky, J. Exp. Theor. Phys. **116**, 780 (2013).
44. E. V. Ganapathy, K. Kugimiya, H. Steinfink, and D. I. Tchernev, J. Less-Common Met. **44**, 245 (1976).
45. I. Goldfarb, F. Cesura, and M. Dascalu, Adv. Mater. **30**, 1800004 (2018).
46. A. J. van Bommel, J. E. Crombeen, and A. van Tooren, Surf. Sci. **48**, 463 (1975).
47. J. N. Hausmann, R. Beltrán-Suito, S. Mebs, V. Hlukhyy, Th. F. Fässler, H. Dau, M. Driess, and P. W. Menezes, Adv. Mater. **33**, 2008823 (2021).
48. D. S. Jensen, S. S. Kanyal, and N. Madaan, Surf. Sci. Spectra **20**, 36 (2013).
49. H.-f. Li, S. Dimitrijev, D. Sweatman, H. Barry Harrison, and Ph. Tanner, J. Appl. Phys. **86**, 4316 (1999).
50. J. H. Kim, J. Y. Yang, J. S. Lee, and J. P. Hong, Appl. Phys. Lett. **92**, 013512 (2008).
51. V. Kinsinger, I. Dezsi, P. Steiner, and G. Langouche, J. Phys.: Condens. Matter **2**, 22 (1990).
52. M. C. Biesinger, B. P. Payne, A. P. Grosvenor, L. W. M. Lau, A. R. Gerson, and R. St. C. Smart, Appl. Surf. Sci. **257**, 2717 (2011).
53. Y. Shin, D. A. Tuan, Y. Hwang, T. V. Cuong, and S. Cho, J. Appl. Phys. **113**, 17C306 (2013).
54. A. Zeleňková, V. Zeleňák, I. Mat'ko, M. Strečková, P. Hrubovčák, and J. Kováč, J. Appl. Phys. **116**, 033907 (2014).
55. S. Bedanta and W. Kleemann, J. Phys. D: Appl. Phys. **42**, 013001 (2009).
56. O. Sendetskyi, L. Anghinolfi, V. Scagnoli, G. Möller, N. Leo, A. Alberca, J. Kohlbrecher, J. Lüning, U. Staub, and L. J. Heyderman, Phys. Rev. B **93**, 224413 (2016).
57. M. Perzanowski, A. Zarzycki, J. Gregor-Pawlowski, and M. Marszalek, ACS Appl. Mater. Interfaces **8**, 28159 (2016).
58. Ch.-Y. Yang, Sh.-M. Yang, Y.-Y. Chen, and K.-Ch. Lu, Nanoscale Res. Lett. **15**, 197 (2020).
59. K. Seo, K. S. K. Varadwaj, P. Mohanty, S. Lee, Y. Jo, M.-H. Jung, J. Kim, and B. Kim, Nano Lett. **7**, 1240 (2007).
60. M. Ziese, I. Vrejoiu, and D. Hesse, Appl. Phys. Lett. **97**, 052504 (2010).
61. V. Asvini, G. Saravanan, R. K. Kalaiezhily, and K. Ravichandran, AIP Conf. Proc. **1942**, 1 (2018).
62. W. Zhu, Zh. Zhu, D. Li, G. Wu, L. Xi, Q. Y. Jin, and Z. Zhang, J. Magn. Magn. Mater. **479**, 179 (2019).
63. I. Goldfarb, F. Cesura, and M. Dascalu, Adv. Mater. **30**, 1800004 (2018).
64. H. Xu, A. C. H. Huan, A. T. S. Wee, and D. M. Tong, Solid State Commun. **126**, 659 (2003).
65. H. Xu, A. C. H. Huan, A. T. S. Wee, and D. M. Tong, J. Appl. Phys. **109**, 023908 (2011).
66. Z. J. Huba, K. J. Carroll, and E. E. Carpenter, J. Appl. Phys. **109**, 07B514 (2011).
67. T. Hasegawa, J. Appl. Phys. Electron. Commun. Jpn. **104**, 2 (2021).
68. M. Belusky, S. Lepadatu, J. Naylor, and M. Vopson, Phys. B (Amsterdam, Neth.) **574**, 411666 (2019).
69. A. M. Lebedev, K. A. Menshikov, V. G. Nazin, V. G. Stankevich, M. B. Tsetlin, and R. G. Chumakov, J. Surf. Invest.: X-ray, Synchrotr. Neutron Tech. **15**, 1039 (2021).

Translated by R. Tyapaev